Broadband Quasi-Phase-Matched Harmonic Generation in an On-Chip Monocrystalline Lithium Niobate Microdisk Resonator

Jintian Lin,[1,*] Ni Yao,[2,*] Zhenzhong Hao,[3] Jianhao Zhang,[1,5] Wenbo Mao,[3] Min Wang,[4] Wei Chu,[1] Rongbo Wu,[1,5] Zhiwei Fang,[4] Lingling Qiao,[1] Wei Fang,[2,†] Fang Bo,[3,‡] and Ya Cheng[1,4,5,6,§]

[1]*State Key Laboratory of High Field Laser Physics, Shanghai Institute of Optics and Fine Mechanics, Chinese Academy of Sciences, Shanghai 201800, China*

[2]*State Key Laboratory of Modern Optical Instrumentation, College of Optical Science and Engineering, Zhejiang University, Hangzhou 310027, China*

[3]*The MOE Key Laboratory of Weak Light Nonlinear Photonics, TEDA Applied Physics Institute and School of Physics, Nankai University, Tianjin 300457, China*

[4]*State Key Laboratory of Precision Spectroscopy, East China Normal University, Shanghai 200062, China*

[5]*University of Chinese Academy of Sciences, Beijing 100049, China*

[6]*Collaborative Innovation Center of Extreme Optics, Shanxi University, Taiyuan, Shanxi 030006, China*

(Received 16 October 2018; published 3 May 2019)

We reveal a unique broadband natural quasi-phase-matching (QPM) mechanism underlying an observation of highly efficient second- and third-order harmonic generation at multiple wavelengths in an x-cut lithium niobate (LN) microdisk resonator. For light waves in the transverse-electric mode propagating along the circumference of the microdisk, the effective nonlinear optical coefficients naturally oscillate periodically to change both the sign and magnitude, facilitating QPM without the necessity of domain engineering in the micrometer-scale LN disk. The second-harmonic and cascaded third-harmonic waves are simultaneously generated with normalized conversion efficiencies as high as 9.9%/mW and 1.05%/mW^2, respectively, thanks to the utilization of the highest nonlinear coefficient d_{33} of LN. The high efficiency achieved with the microdisk of a diameter of ~30 μm is beneficial for realizing high-density integration of nonlinear photonic devices such as wavelength convertors and entangled photon sources.

DOI: 10.1103/PhysRevLett.122.173903

With the rapid development of micro- and nanofabrication techniques, lithium niobate on an insulator (LNOI) has emerged to become a promising candidate for an integrated photonic platform [1–13]. Its excellent nonlinear optical property combined with the capacity of fabricating high-quality LNOI photonic structures has triggered significant interest to achieve efficient wavelength conversion in various types of photonic devices such as microdisks [14–18], microrings [19–21], and periodically poled LN (PPLN) waveguides [22]. Among them, high-quality (Q) factor microdisks are promising candidates as these devices can operate at any wavelengths in the transmission spectrum and be fabricated to have smooth boundaries for supporting low optical losses [8–21,23]. However, efficient wavelength conversion in microdisks poses a challenging task due to the lack of flexible control on the dispersion to satisfy the stringent phase-matching condition [24]. Meanwhile, the birefringence of the LN crystal often makes it difficult to choose the largest nonlinear coefficient d_{33} when attempting to realize phase-matched nonlinear processes. In this Letter, we report highly efficient second- and third-harmonic generation (SHG and THG, respectively) in a high-Q x-cut LN microdisk based on natural QPM. We characterize the transmission spectra and perform theoretical simulations to reveal the involved mechanism which nicely explains all the observed phenomena.

In the fabrication of the LN microdisk resonator, an x-cut LNOI wafer (NANOLN, Jinan Jingzheng Electronics Co., Ltd) was used. The top LN film has a thickness of 600 nm, which is bonded to a silica buffer layer of 2 μm thickness deposited on a 500-μm-thick LN substrate. After patterning the LNOI into the disk with femtosecond-laser ablation, polishing the sidewall with focused ion beam milling, and undercut etching of fused silica beneath the LN microdisk in a diluted HF solution [14], a freestanding LN microdisk with a diameter of 29.92 μm was fabricated, as shown in Fig. 1(a). The enlarged scanning electron microscope (SEM) image shown in Fig. 1(b) indicates a smooth sidewall with a small tilt angle of approximately 10°.

The experimental setup for investigating the nonlinear optical processes was schematically illustrated in Fig. 1(c), in which a tunable diode laser (Model 688-LN, New Focus Inc.) amplified by an erbium-ytterbium-doped fiber amplifier (EDFA) was used as the pump light source. The laser was launched into a SM-28 single mode fiber, and the pump light was coupled to the microdisk via the fiber taper with a diameter of 900 nm [25]. An inline polarization

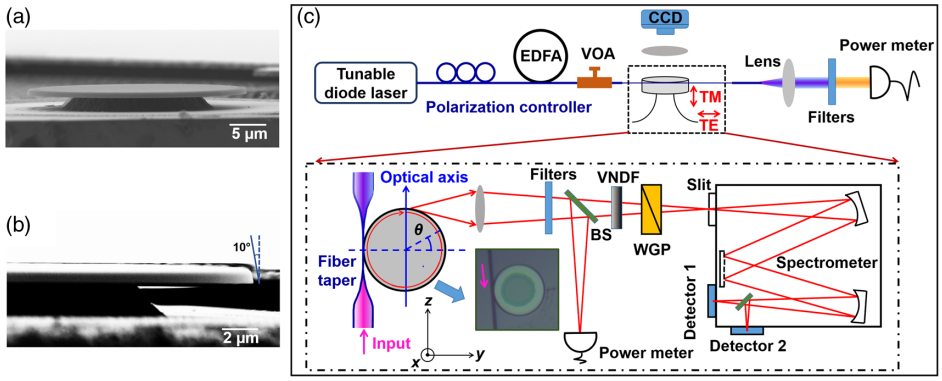

FIG. 1. (a) SEM image of the microresonator. (b) The side-view SEM image of the microresonator. (c) Experimental setup of nonlinear optical processes in the microresonator. Inset: Experimental setup for determining the polarization properties and recording the spectrum and power by collecting the scattering light from the edge of the microresonator. Here, beam splitter is BS for short.

controller was used to ensure the excitation of TE modes in the LN microdisk.

The inset in Fig. 1(c) shows the schematic diagram of the setup for measuring the spectra and powers of SHG and THG signals. An objective lens with numerical aperture (NA) of 0.25 was used to collect the emission light from the side of the microdisk. A silicon detector array and an InGaAs detector array were mounted on the spectrometer (SR303i, Andor Inc.) to measure the harmonic signals and the pump light, respectively. To verify the polarization states of resonant modes in the microresonator, a calibrated wire grid polarizer (WGP) was also inserted. A set of filters (see Supplemental Material, Sec. S1 [26], for details) were used when measuring the spectra of different signals.

In our experiments, when the pump laser wavelength was tuned to 1547.8 nm and the in-coupled power was set at 0.25 mW, a bright visible emission from the LN microdisk could be spotted by the eye. The spectra of the pump laser and the second-harmonic wave at 773.9 nm are shown in Fig. 2(a), both of which are confirmed to be TE polarized. From the CCD camera, the second-harmonic beam is clearly visible around the circumference of the LN microdisk, as shown in the inset in Fig. 2(b). The measured conversion efficiency grows linearly with the increasing pump power with a normalized conversion efficiency of 9.9%/mW in the LN microdisk, as shown in Fig. 2(b). Specifically, the pump power used in the calculation is the in-coupled power, which has taken into account the coupling factor of 62.2% (defined by measuring the resonance "dip" contrast in the linear regime). Moreover, it should be noted that the signal (second- or third-harmonic) power depends on the signal collection efficiency of the lens. In our experiment, the objective lens used for collecting the signals has a NA of 0.25, resulting in a low collection efficiency of 3.98% for the second- and third-harmonic signals. The total powers of second- and third-harmonic signals used in the calculation of the normalized conversion efficiency have been calibrated with the collection efficiency of the lens. We notice that, previously, the best results of the normalized conversion efficiency of SHG achieved in LNOI-based nanophotonic structures (i.e., microdisks, microrings, and waveguides) are all on the order of 10^{-3}/mW [16,22,29]. Thus, the result obtained using the natural QPM in our experiment is at least one order of magnitude higher than the best results reported before.

When the pump laser power was further increased, resonant emission at the third-harmonic wavelength [515.9 nm; see Fig. 2(a)] was observed from the CCD camera, as shown in the inset in Fig. 2(c). The bright green emission could also be observed by the eye at the in-coupled power of 0.37 mW. Again, the third-harmonic wave was TE polarized. The output power of the third-harmonic signal is plotted as a function of the

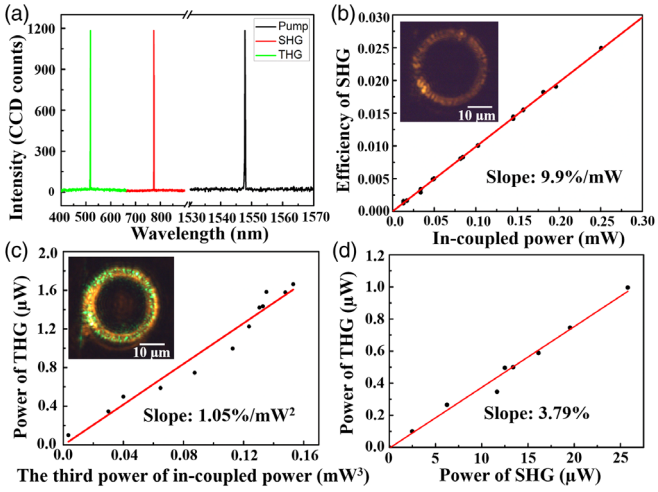

FIG. 2. (a) Spectra of the pump light, the second-harmonic wave, and the third-harmonic wave. (b) Conversion efficiency of SHG as a function of the in-coupled power. Inset: Top-view optical micrograph of the SHG from the microresonator. (c) The power of cascaded THG as a function of the cubic power of the in-coupled light. Inset: Top-view image of the cascaded THG. (d) The power of the cascaded THG as a function of the power of the second harmonic.

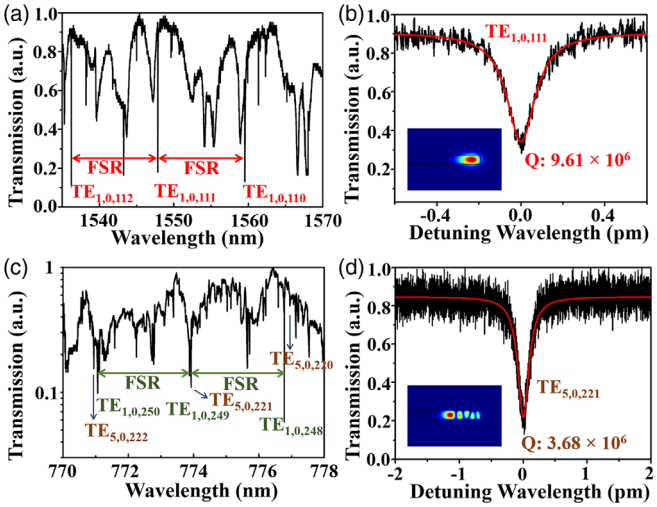

FIG. 3. (a) Transmission spectrum around the pump wavelength. (b) Q factor of the $TE_{1,0,111}$ mode, which is 9.61×10^6. (c) Transmission spectrum around the second-harmonic wavelength. (d) Q factor of the $TE_{5,0,221}$ mode, which is 3.68×10^6.

in-coupled power in Fig. 2(c), indicating a normalized conversion efficiency of $1.05\%/\mathrm{mW}^2$ from the pump light. This is almost 6 orders of magnitude higher than the conversion efficiency demonstrated with a fan-out periodically poled resonator [30]. Figure 2(d) shows a linear growing slope of 3.79% in the cascaded THG power with the increasing second-harmonic signal.

Remarkably, the efficient SHG and THG processes in the LN microdisk are not peculiar to a certain wavelength. When the pump laser wavelength was scanned from 1530 to 1570 nm, strong second-harmonic and third-harmonic signals appeared at several wavelengths. For example, when the pump laser wavelength was at 1562.3 nm, the second- and third-harmonic signals were measured to have normalized conversion efficiencies of $10.0\%/\mathrm{mW}$ and $2.79\%/\mathrm{mW}^2$, respectively.

The resonant modes involved in the nonlinear processes were identified by measuring the transmission spectra around the fundamental and second-harmonic wavelengths via the fiber taper coupling method [31]. The details can be found in Supplemental Material, Sec. S2 [26]. Figures 3(a) and 3(c) show the respective transmission spectra, from which the fundamental mode at 1547.8 nm was identified as $TE_{1,0,111}$ WGM and the SHG mode at 773.9 nm was identified as $TE_{5,0,221}$ WGM. Here we used three subscripts to denote the mode number, other than four subscripts. The first number "1" indicates the radial mode number, the second number "0" indicates the polar-mode number, and the third number "111" indicates the azimuthal mode number. The Q factors of the $TE_{1,0,111}$ mode and $TE_{5,0,221}$ mode were determined to be 9.61×10^6 and 3.68×10^6, respectively, by Lorentz fittings of the resonant dips as shown in Figs. 3(b) and 3(d). When the pump wavelength was set as 1547.8 or 1562.3 nm, the coupling factor of the pump power into the microresonator was 62.2% or 24.3%, respectively.

We now perform theoretical analyses of the results. In an x-cut LN microdisk, the TE wave traveling around the circumference experiences a rotating crystal orientation, as the optical axis of the crystal is along the z direction. The effect gives rise to the variations of both the nonlinear coefficient and the refractive index along the periphery of the LN microdisk. The second-order nonlinear coefficient can be expressed as

$$d_{\mathrm{eff}} = -d_{22}\cos^3\theta + 3d_{31}\cos^2\theta\sin\theta + d_{33}\sin^3\theta, \qquad (1)$$

where θ is the angle between the wave vector $\boldsymbol{k}$ of the TE-polarized wave and the optical axis, indicated as the azimuth angle in Fig. 4(a). Figure 4(b) plots the dependence

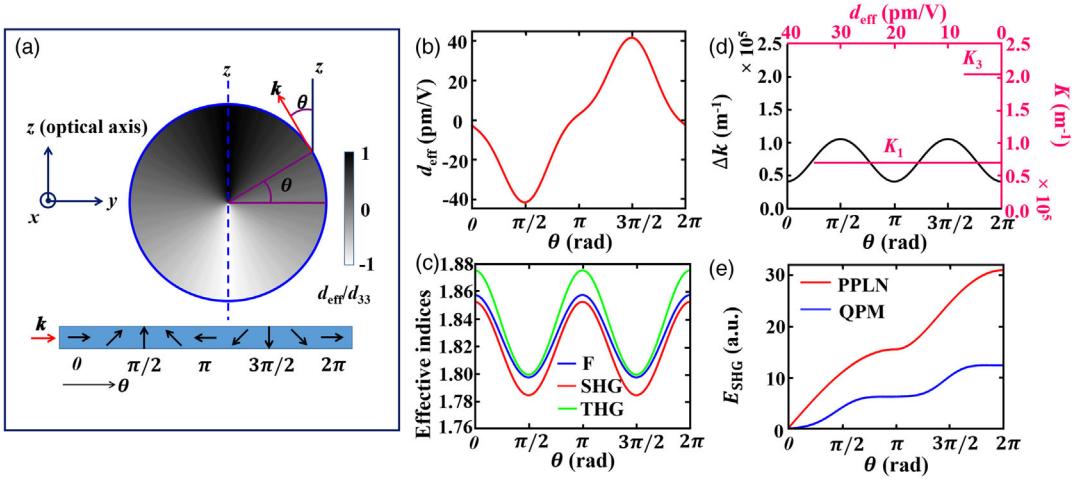

FIG. 4. (a) The variations of d_{eff} of a TE-polarized wave are schematically illustrated in an x-cut LN microresonator. (b) d_{eff} at every azimuth angle θ. (c) Effective refractive indices at every θ. (d) Left: Phase mismatching Δk; right: the positive Fourier components of d_{eff}. (e) The growth of E_{SHG} versus θ along the microresonator periphery (blue line), while the red line is that of the fan-out PPLN microdisk.

of d_{eff} on θ, which clearly shows that the sign of d_{eff} inverts every half cycle in the LN microdisk as illustrated in Fig. 4(a). This is analog to the periodic domain inversion in a PPLN crystal. One can introduce an additional $\boldsymbol{k}$ vector for compensating the phase mismatch between the optical modes, giving rise to efficient nonlinear processes.

Likewise, the effective refractive indices of the fundamental and second-harmonic modes also experience periodic variations along the periphery, as shown in Fig. 4(c), in which both the material and geometry dispersion have been taken into account. It is known that, for a quasi-phase-matched SHG in a PPLN crystal, the wave vector mismatching Δk should fulfill the following condition [32]:

$$\Delta k = 2k_F - k_{\mathrm{SHG}} = mK_i, \tag{2}$$

where k_F and k_{SHG} are the wave vectors of the fundamental and the second-harmonic waves, respectively, K_i is the ith Fourier component of d_{eff} in the wave vector space, and m is an integer. As both k_F and k_{SHG} are constants in the conventional PPLN crystal, the spatial period of PPLN therefore has to be discrete values which are determined by the operating wavelength. For this reason, broadband nonlinear wavelength conversion in a PPLN crystal requires elaborate designs of the domain patterns [33,34], while in the LN microdisk, Δk is no longer a constant but oscillates within a certain range, which allows multiple choices of K_i to fulfill the quasi-phase-matching condition.

In our case, for $\mathrm{TE}_{1,0,111}$ and $\mathrm{TE}_{5,0,221}$ modes, the respective k_F and k_{SHG} were estimated by $k = 2\pi n_{\mathrm{eff}}/\lambda$. The calculated Δk was plotted in Fig. 4(d) as represented by an oscillating curve between 0.406×10^5 and $1.055 \times 10^5\ \mathrm{m}^{-1}$. K_i can be calculated by performing a Fourier transform of d_{eff} with respect to the propagation distance $s = r\theta$, where $r = 14.66\ \mu\mathrm{m}$ is the radius of the maximum of the fundamental-wave electric field. As K_1 was calculated to be $0.682 \times 10^5\ \mathrm{m}^{-1}$, which falls into the oscillation range of Δk, the QPM condition was satisfied and efficient SHG was observed.

To further prove it, the periodic growth of the second-harmonic signal can be calculated numerically in a full cycle. The electric field profiles of $\mathrm{TE}_{1,0,111}$ and $\mathrm{TE}_{5,0,221}$ modes were first calculated via the finite-element simulation method (details can be found in Supplemental Material, Sec. S3) [26], as shown in the insets in Figs. 3(b) and 3(d), respectively. Under the slowly varying amplitude approximation, the growth rate of the field amplitude E_{SHG} of the second-harmonic wave with the varying θ can be expressed as [16,35]

$$\frac{dE_{\mathrm{SHG}}}{ds} = \frac{id_{\mathrm{eff}}\omega_{\mathrm{SHG}}^2}{k_{\mathrm{SHG}}c^2} E_F^2 e^{i\int \Delta k ds} - \frac{E_{\mathrm{SHG}}}{2k_{\mathrm{SHG}}} \times \frac{dk_{\mathrm{SHG}}}{ds}, \tag{3}$$

where $ds = rd\theta$. In Eq. (3), ω_{SHG} and E_F are the angular frequency of the second harmonic and the field amplitude of the fundamental wave, respectively. Figure 4(e) shows how the field amplitude of the second-harmonic signal E_{SHG} grows within the first cycle [blue line in Fig. 4(e)]. For comparison, the growth of E_{SHG} in an ideal (i.e., lossless) fan-out PPLN microdisk is also plotted (red line). Although the calculated conversion efficiency in the fan-out PPLN microdisk is twice as high as that in our x-cut LN microdisk, it should be noted that the micropoling process typically introduces a non-negligible loss [18].

As the third-order nonlinear coefficient of LN material is small, the bright third-harmonic signal at 515.9 nm comes from the cascaded process by a sum-frequency generation between the second-harmonic and fundamental waves [36]. Thanks to the broadband characteristic of our phase-matching mechanism, the QPM condition is still maintained as clarified by our simulation results (Supplemental Material, Sec. S4 [26]). Thus, by choosing an x-cut LN wafer and TE-polarized modes, nonlinear wavelength conversion processes with ultrahigh efficiencies over a broad wavelength range have been achieved.

The work is supported by NSFC (Grants No. 11734009, No. 61590934, No. 61635009, No. 61327902, No. 11604351, No. 11674340, No. 11674181, and No. 11874375); Key Research Program of Frontier Sciences, CAS (Grant No. QYZDJ-SSW-SLH010); Key Project of the Shanghai Science and Technology Committee (Grants No. 18DZ1112700 and No. 17JC1400400); Shanghai Rising-Star Program (Grant No. 17QA1404600); and the Fundamental Research Funds for the Central Universities (Grant No. 2018FZA5004).

*These authors contributed equally to this work.
†wfang08@zju.edu.cn
‡bofang@nankai.edu.cn
§ya.cheng@siom.ac.cn

[1] G. Poberaj, H. Hu, W. Sohler, and P. Günter, Laser Photonics Rev. **6**, 488 (2012).
[2] A. Boes, B. Corcoran, L. Chang, J. Bowers, and A. Mitchell, Laser Photonics Rev. **12**, 1700256 (2018).
[3] R. Wu, M. Wang, J. Xu, J. Qi, W. Chu, Z. Fang, J. Zhang, J. Zhou, L. Qiao, Z. Chai, J. Lin, and Y. Cheng, Nanomaterials **8**, 910 (2018).
[4] C. Wang, M. Zhang, X. Chen, M. Bertrand, A. Shams-Ansari, S. Chandrasekhar, P. Winzer, and M. Lončar, Nature (London) **562**, 101 (2018).
[5] J. E. Toney, *Lithium Niobate Photonics* (Artech House, Boston, 2015).
[6] H. Jin, F. M. Liu, P. Xu, J. L. Xia, M. L. Zhong, Y. Yuan, J. W. Zhou, Y. X. Gong, W. Wang, and S. N. Zhu, Phys. Rev. Lett. **113**, 103601 (2014).
[7] N. G. R. Broderick, G. W. Ross, H. L. Offerhaus, D. J. Richardson, and D. C. Hanna, Phys. Rev. Lett. **84**, 4345 (2000).

[8] V. S. Ilchenko, A. A. Savchenkov, A. B. Matsko, and L. Maleki, Phys. Rev. Lett. **92**, 043903 (2004).
[9] J. U. Fürst, D. V. Strekalov, D. Elser, M. Lassen, U. L. Andersen, C. Marquardt, and G. Leuchs, Phys. Rev. Lett. **104**, 153901 (2010).
[10] J. U. Fürst, D. V. Strekalov, D. Elser, A. Aiello, U. L. Andersen, Ch. Marquardt, and G. Leuchs, Phys. Rev. Lett. **105**, 263904 (2010).
[11] J. U. Fürst, D. V. Strekalov, D. Elser, A. Aiello, U. L. Andersen, Ch. Marquardt, and G. Leuchs, Phys. Rev. Lett. **106**, 113901 (2011).
[12] M. Förtsch, J. U. Fürst, C. Wittmann, D. Strekalov, D. Strekalov, A. Aiello, M. V. Chekhova, C. Silberhorn, G. Leuchs, and C. Marquardt, Nat. Commun. **4**, 1818 (2013).
[13] J. Moore, M. Tomes, T. Carmon, and M. Jarrahi, Appl. Phys. Lett. **99**, 221111 (2011).
[14] J. Lin, Y. Xu, Z. Fang, M. Wang, J. Song, N. Wang, L. Qiao, W. Fang, and Y. Cheng, Sci. Rep. **5**, 8072 (2015).
[15] J. Wang, F. Bo, S. Wan, W. Li, F. Gao, J. Li, G. Zhang, and J. Xu, Opt. Express **23**, 23072 (2015).
[16] J. Lin, Y. Xu, J. Ni, M. Wang, Z. Fang, L. Qiao, W. Fang, and Y. Cheng, Phys. Rev. Applied **6**, 014002 (2016).
[17] R. Luo, H. Jiang, S. Rogers, H. Liang, Y. He, and Q. Lin, Opt. Express **25**, 24531 (2017).
[18] Z. Hao, L. Zhang, A. Gao, W. Mao, X. Lyu, X. Gao, F. Bo, F. Gao, G. Zhang, and J. Xu, Sci. China-Phys. Mech. Astron. **61**, 114211 (2018).
[19] R. Wolf, Y. Jia, S. Bonaus, C. S. Werner, S. J. Herr, I. Breunig, K. Buse, and H. Zappe, Optica **5**, 872 (2018).
[20] R. Wolf, I. Breunig, H. Zappe, and K. Buse, Opt. Express **25**, 29927 (2017).
[21] R. Luo, Y. He, H. Liang, M. Li, and Q. Lin, Optica **5**, 1006 (2018).
[22] C. Wang, C. Langrock, A. Marandi, M. Jankowski, M. Zhang, B. Desiatov, M. M. Fejer, and M. Lončar, Optica **5**, 1438 (2018).
[23] R. Wu, J. Zhang, N. Yao, W. Fang, L. Qiao, Z. Chai, J. Lin, and Y. Cheng, Opt. Lett. **43**, 4116 (2018).
[24] I. Breunig, Laser Photonics Rev. **10**, 569 (2016).
[25] Y. Xu, W. Fang, and L. Tong, Opt. Express **25**, 10434 (2017).
[26] See Supplemental Material http://link.aps.org/supplemental/10.1103/PhysRevLett.122.173903 for the simulations of mode distribution, which includes Refs. [27,28].
[27] M. Oxborrow, IEEE Trans. Microw. Theory Technol. **55**, 1209 (2007).
[28] M. V. Hobden and J. Warner, Phys. Lett. **22**, 243 (1966).
[29] J. Moore, J. K. Douglas, I. W. Frank, T. A. Friedmann, R. Camacho, and M. Eichenfield, in *Conference on Lasers and Electro-Optics, OSA Technical Digest (online)* (Optical Society of America, 2016), p. STh3P.1.
[30] K. Sasagawa and M. Tsuchiya, Appl. Phys. Express **2**, 122401 (2009).
[31] J. C. Knight, G. Cheung, F. Jacques, and T. A. Birks, Opt. Lett. **22**, 1129 (1997).
[32] D. D. Hickstein, D. R. Carlson, A. Kowligy, M. Kirchner, S. R. Domingue, N. Nader, H. Timmers, A. Lind, G. G. Ycas, M. M. Murnane, H. C. Kapteyn, S. B. Papp, and S. A. Diddams, Optica **4**, 1538 (2017).
[33] T. Beckmann, H. Linnenbank, H. Steigerwald, B. Sturman, D. Haertle, K. Buse, and I. Breunig, Phys. Rev. Lett. **106**, 143903 (2011).
[34] D. Haertle, J. Opt. **12**, 035202 (2010).
[35] G. Lin, J. U. Fürst, D. V. Strekalov, and N. Yu, Appl. Phys. Lett. **103**, 181107 (2013).
[36] S. Zhu, Y. Zhu, and N. Ming, Science **278**, 843 (1997).